MATERIALS ANALYSIS OF TRANSIENT PLASMA-WALL INTERACTIONS

JOHN SLOUGH
UNIVERSITY OF WASHINGTON

05/13/2014
Final Report

REPORT DOCUMENTATION PAGE

Form Approved
OMB No. 0704-0188

1. REPORT DATE *(DD-MM-YYYY)* 05-12-2014	2. REPORT TYPE Final	3. DATES COVERED *(From - To)* June 15, 2011 - Mar 14, 2014

4. TITLE AND SUBTITLE	5a. CONTRACT NUMBER
Title: Materials Analysis of Transient Plasma-Wall Interactions Subtitle: Final Performance Report	**5b. GRANT NUMBER** AFOSR FA9550-11-1-0097
	5c. PROGRAM ELEMENT NUMBER

6. AUTHOR(S)	5d. PROJECT NUMBER
John Slough and Fumio Ohuchi	**5e. TASK NUMBER**
	5f. WORK UNIT NUMBER

7. PERFORMING ORGANIZATION NAME(S) AND ADDRESS(ES)	8. PERFORMING ORGANIZATION REPORT NUMBER
University of Washington Dept. of Aeronautics and Astronautics Box 352400 University of Washington, Seattle, WA 98195	62-2598 Final Report

9. SPONSORING / MONITORING AGENCY NAME(S) AND ADDRESS(ES)	10. SPONSOR/MONITOR'S ACRONYM(S)
Dr. Mitat A. Birkan AFOSR/RTE (703) 696-7234 DSN 426-7234; FAX (703) 696-7320 E-mail: mitat.birkan@us.af.mil	**11. SPONSOR/MONITOR'S REPORT NUMBER(S)**

12. DISTRIBUTION / AVAILABILITY STATEMENT

DISTRIBUTION STATEMENT A. Approved for public release; distribution is unlimited.

13. SUPPLEMENTARY NOTES

14. ABSTRACT

This program seeks to advance the field of high temperature materials, space propulsion and electro-energetic physics research. With the discovery of a new class of electromagnetic pulsed plasma propulsion devices such as the Electrodeless Lorentz Force Thruster, it is critical to characterize and develop and new materials for these systems. Through a combination of experiment and surface analysis, the behavior of the plasma-material boundary under transient thermal convective and radiative loads was investigated. Specifically, transient non-equilibrium plasma flows have been produced over a range of high energy densities (100 kJ/m2 – 500 kJ/m2), on time scales of 10s of microseconds. The initial investigations employed deuterium plasmas to reduce the effect of radiation effects while providing for a chemically active species whose effect on the substrate could easily be traced. The chemical and physical effects of these flows on a range of insulative, conducting and composite materials were examined by detailed surface analysis on the micro, meso and macro scale. The information obtained through Optical Microscopy, Secondary Electron Microscopy, and X-ray Photoelectron Spectroscopy were used to develop a model showing the importance sputter and re-deposition.

15. SUBJECT TERMS

plasma, pulsed plasma, directed energy, transient wall interaction, high energy density, optical microscopy, secondary electron

16. SECURITY CLASSIFICATION OF:			17. LIMITATION OF ABSTRACT	18. NUMBER OF PAGES	19a. NAME OF RESPONSIBLE PERSON Prof. John Slough
a. REPORT U	**b. ABSTRACT** U	**c. THIS PAGE** U	UU		**19b. TELEPHONE NUMBER** *(include area code)* (425) 867-8900

Standard Form 298 (Rev. 8-98)
Prescribed by ANSI Std. Z39.18

Materials Analysis of Transient Plasma-Wall Interactions

Final Performance Report

AFOSR FA9550-11-1-0097

PI: John Slough
Plasma Dynamics Laboratory
University of Washington

Co-PI: Fumio Ohuchi
Department of Materials Science and Engineering
University of Washington

Co-PI: Richard Milroy
Plasma Science and Innovation (PSI) Center
University of Washington

DuWayne L. Smith[1], Samuel Andreason[2], Chris Pihl[2]

[1] *Department of Materials Science & Engineering*

[2] *Department of Aeronautics & Astronautics, Plasma Dynamic Lab,*

University of Washington

Seattle, WA, 98195

May, 12, 2014

1

I. PROJECT SUMMARY

Recent investigations into the chemical and physical dynamics of plasma produced inside the reactor cores have revealed a significant problem with the stability of materials used in plasma facing positions. In particular, materials exposed to transient non-equilibrium, chemically reactive, highly magnetized plasmas experience a high rate of erosion resulting in a number of undesirable effects [1 2 3]. Among these effects are physical and chemical sputtering and re-deposition [4], chemical contamination of plasma due to chamber wall erosion [5, 6], and chemical adsorption of fuel gasses at the wall surface [7, 8]. These effects greatly reduce the operational reliability and lifetime of devices that rely on plasma reactor chambers as their principal components. Our research of this Phase-I program was to focus on investigating the transient non-equilibrium plasma flows and their interactions with various materials.

In order to make these studies during 2.5 years of the project, we have built two new high-power transient plasma facilities dedicated to the investigation of plasma-wall interactions. The first system was designed and assembled using existing facilities at the Plasma Dynamics Laboratory at the University of Washington. This is briefly described in the EXPERIMENTAL FACILITY (section **II.a**), and has been operated for the first 1.5 years, generating results described in **III.a**, **III.b**, **III.c** and **III.d** in the **RESULTS** section. The second system was built during the second year to better characterize the plasma, which is described in **II.b-II.h** in the **EXPERIMENTAL FACILITY** section in detail. The design and characteristics of this facility has been recently submitted to *Review of Scientific Instruments*. Preliminary results of the plasma-wall interactions using this second facility has been described in **III.e** in the **RESULTS** section.

Studies pursued during the funded period focused on two broad areas of interest; (1) the effects of the chamber geometry on sputtering and re-deposition, and (2) the effect of chemical, morphological and structural changes resulting directly from the exposures to the transient components of pulsed plasmas. While our long range goal is to investigate a variety of plasma fuel gasses, from Hydrogen through Xenon, our preliminary studies involve the use of high density deuterium plasma with an average fluence on the order of $1\sim10kJ/m^2$. The primary materials to be tested were metals (such as copper, aluminum, zirconium, titanium, and tungsten) and ceramics (beryllia, aluminum nitride, silicon carbide, etc.). These materials were chosen for their intrinsic properties such as electrical and thermal conductivity, hardness, and resistance to sputtering, and resistance to ion and neutron implantation. In addition Macor® was used as a material to hold these materials during the exposures for its insulating properties, low thermal conductivity and coefficient of thermal expansion, as well as chemical stability and composition. The composition of Macor® is known to include silicon, magnesium, aluminum, potassium, boron, and fluorine [8]. With the exception of fluorine, all other elements present in Macor® are in oxidized forms, therefore, by employing Macor® as a sample holder, we were able to introduce a ceramic sample with a variety of constituent elements together with metals for chemical analysis during our exposures. General procedures for Materials Characterization were described in **II.h**.

The **RESULTS** section consists of investigations of compositional changes of the Macor® surface induced by D_2 plasma irradiation in (**III.a**). Effects of geometry on the sputter and re-deposition dynamics during pulsed plasma exposures were conducted by setting the tungsten (W) specimens in the Macor® sample holder at varying heights and depths relative to the holder surface (**III.b**). The chemical and morphological interactions between plasma and variety of sample materials (Cu, Ti, Zr, and W) are describe in (**III.c**). The structural variation of ceramic samples

(BeO) before and after plasma irradiation are investigated in (**III.d**). And preliminary results from the newly developed plasma facility are described in (**III.e**).

II. EXPERIMENTAL FACILITY

II.a Plasma facility for initial study

In the first 1.5 years of research, an experimental facility to investigate the transient plasma interactions with test specimens was designed and assembled using existing facilities at the Plasma Dynamics Laboratory at the University of Washington. To make it operational for the transient plasma/materials interaction studies, the Field Reversed Configuration (FRC) plasmoid was generated from the magnetic compression of an existing highly ionized and uniform Rotating Magnetic Fields (RMF) plasma. This is shown in Fig. 1.
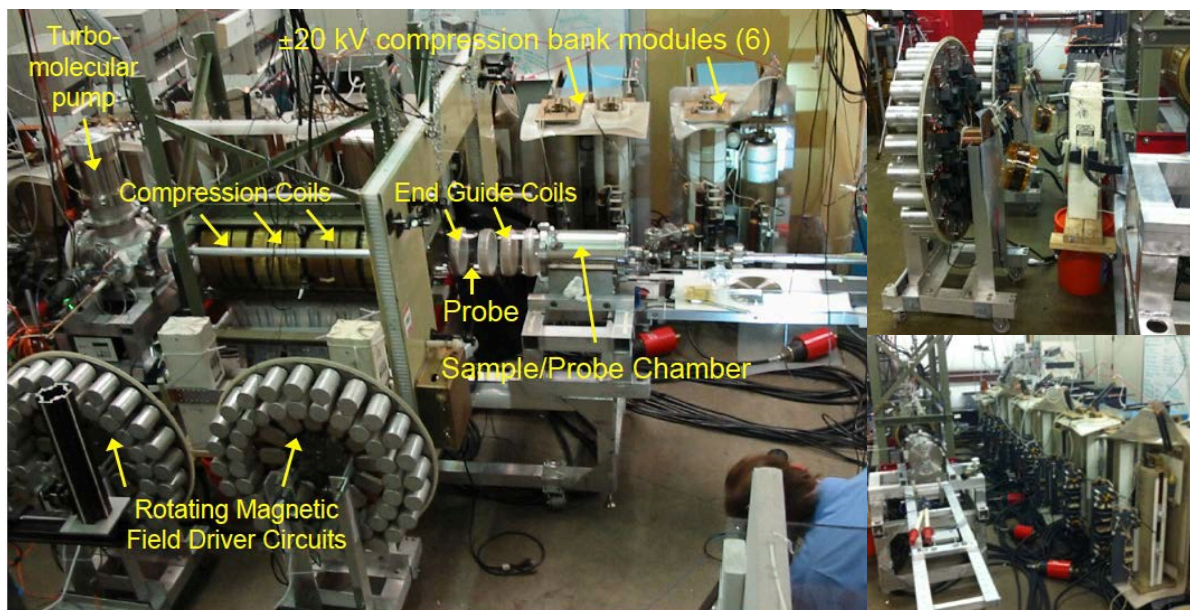

Figure 1: Photographs showing the FRC plasma experimental test bed used for the transient plasma/materials interaction studies (left), RMF energy storage consisting of 84-1mF/450V electrolytic capacitors (right top), and theta pinch energy storage consisting of 30-14.1 µF/25kV pulse capacitors (right bottom)

With this plasma formation and sustainment technique alone, a plasma jet having a kinetic energy density fluence on target ranging from 8 to 40 kJ/m^2 was realized. This device equips a set of 3-turn theta pinch coils energized with a 90 kJ, 20 kV pulse power capacitor bank, with which the RMF plasma was rapidly compressed to increase the plasma energy, and hence target energy fluence as much as up to a factor of 30 times that of the RMF system was obtained. The device was thus capable of a wide range of transient plasma conditions for study. These include pulse durations from a few microseconds to several milliseconds with a plasma jet having a kinetic energy fluence on target ranging from 1 kJ/m^2 to 1 MJ/m^2 making possible a transient materials exposure spanning the range from the smallest thruster to the largest fusion energy or directed energy devices.

The evaluation of the FRC plasma energy was readily obtained from external magnetic loop measurements. It was observed that this plasma energy flew out axially over the lifetime of the FRC (10 - 50 microseconds) and impinges on the samples placed in and azimuthal array at a radius of ~ 1 cm. This assures that they are all exposed equally to the plasma jet that extends out radially ~ 2 cm at the axial location of the samples as shown in Fig. 2.

II.b Newly designed and constructed plasma facility and preliminary results

A Field Reversed Configuration (FRC) plasma source was designed and constructed to conduct high energy plasma-materials interaction studies. The purpose of these studies is the development of advanced materials for use in plasma based electric propulsion systems. Outlined within this paper is the basic concept of FRC plasmoid creation, an overview of the device design and the integration of plasma characterization and diagnostics systems. Using a Michelson interferometer it was determined that the FRC plasma densities

Figure 2. **A photograph showing the plasma jet extending out radially at the axial location of the sample surface.**

are on the order of ~10^{21} m^{-3}. A novel dynamic pressure probe was created to measure ion velocities averaging 300 km/s. Compensating flux loop arrays were used to measure magnetic field strength and verify the existence of the FRC plasmoid and when used in combination with density measurements it was determined that the average ion temperatures are ~130 eV. X-ray Photoelectron Spectroscopy (XPS) was employed as a means of characterizing the size and shape of the plasma jet in the sample exposure position. It was determined that the plasma jet is roughly 1.2 cm in diameter.
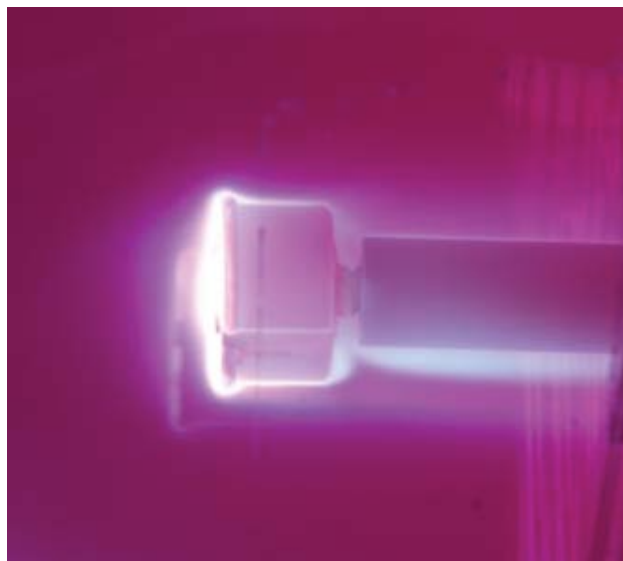
II.c Background

Over the past 20 years the study of plasma-materials interactions have been validated through countless modern processing techniques that utilize the high energy, dimensionality and chemical reactivity of plasmas to create some of the most technically advanced tools in existence today. From plasma etching of microchips to the promise of fusion based pulsed power systems, plasma science will continue to evolve as a fundamental and highly specialized field with broad ranging applications. Because of the complexity of plasma-materials interactions, which often encompass the interaction of matter in four different states, it is of great importance that a reliable test bed be used to conduct such studies [9]. The ability to accurately and efficiently characterize plasma dynamics and energies in relation to physical and chemical mutations of solids resulting directly from ion exposures is crucial to the development of plasma devices and processing techniques.

The program at the University of Washington that combines the expertise of plasma physics and materials science researchers has been developed that seeks to advance the field of high

temperature materials, space propulsion and electro-energetic physics research. With the discovery of a new class of electromagnetic pulsed plasma propulsion devices such as the Electrodeless Lorentz Force (ELF) Thruster [10], it is critical to characterize and develop new materials for these systems that can withstand the demanding conditions of space propulsion and directed energy. It was realized that a small system would be best suited for a fast, efficient and highly characterized plasma source. The interaction studies require plasma fluence conditions to be in the range of kJ/m^2 to MJ/m^2 for significant relatable material damage to occur. It was concluded that a small scale Field Reversed Configuration (FRC) plasma source [11] could generate a sufficiently dense and energetic plasma jet to be directed at material samples in order to conduct interaction studies.

An FRC is a compact toroid characterized by its inherent high plasma β (the ratio of the internal plasma pressure to the external magnetic field pressure), simply connected topology and a purely poloidal field [3]. FRC's are well studied [12], and commonly yield plasma densities on the order of $\sim 10^{21}$ m^{-3} and can be translated with plasmoid velocities $\sim 10^5$ m/s [13]. Not only is the plasma source critical to the success of these studies, but the most accurate characterization of plasma conditions at the surface of the material sample is at the center of our focus. It was therefore necessary to build a device specifically tailored for highly accurate plasma diagnostics. A
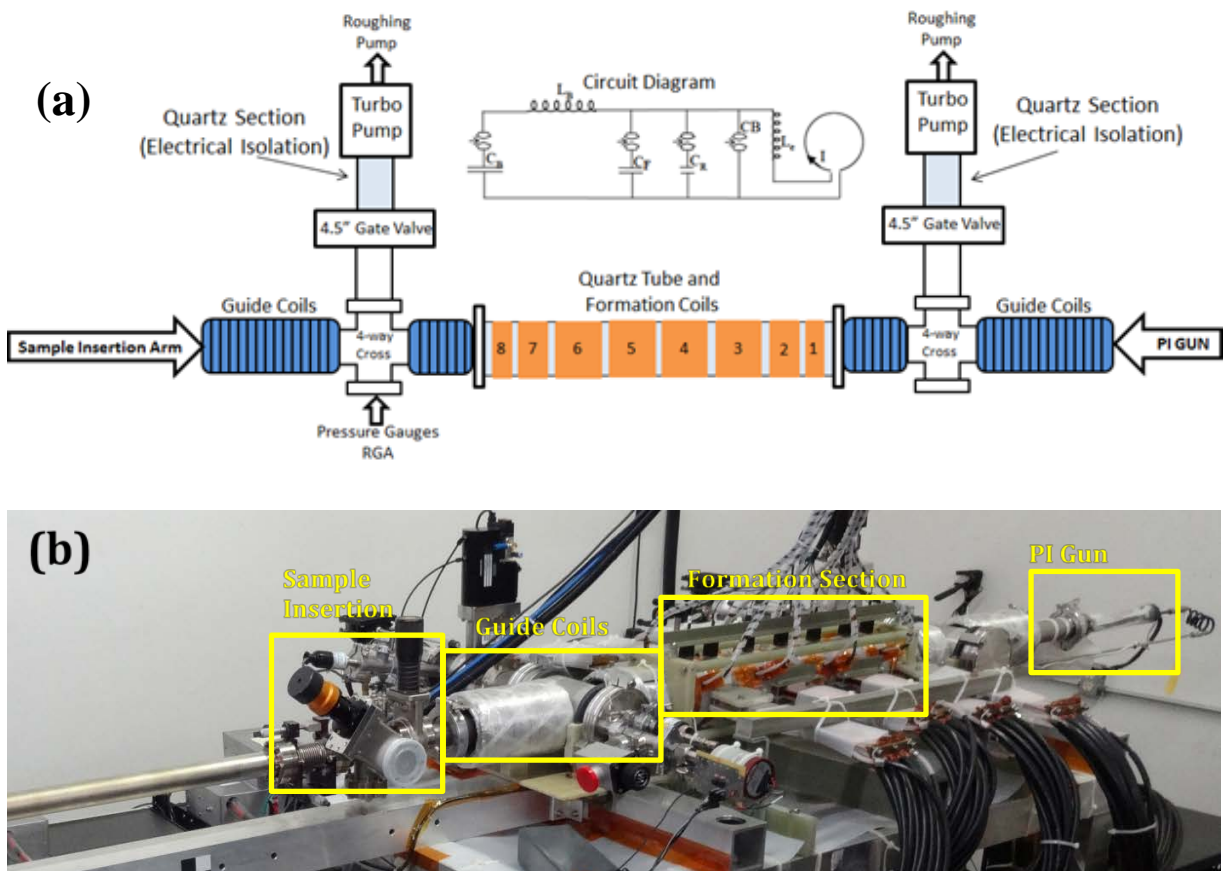

Figure 3. (a) **Illustrates the top down view and layout of the FRC chamber with supporting vacuum system including the circuit diagram for each coil in the formation section. (b) Fully assembled and operational Field Reversed Configuration plasma source designated as plasma-materials interactions studies test bed.**

5

Michelson Interferometer was used to measure plasma densities, a series of wire loops acting as compensating flux arrays were attached to each coil to accurately measure field strengths and excluded flux profiles during FRC formation. A novel dynamic pressure probe was created to measure ion velocities within the plasma jet. As well, X-ray Photoelectron Spectroscopy (XPS) was employed as a means of elucidating the finer structure of the plasma jet. This paper seeks to outline the general concept of FRC plasmoid formation as well as the overall design and integration of the plasma source with diagnostics and sample exposure stage. The compact and efficient design of the device discussed in this report has proven to be most reliable, gives highly consistent shot-to-shot plasma conditions, and will serve as an excellent test bed for future plasma material interaction studies.

II.d Design and Construction

The basic concept of an FRC plasma source involves the creation of a closed magnetic field profile that effectively traps and compresses an ionized gas into an ellipsoid structure known as a "plasmoid". The plasmoid has a lifetime governed by the L/R decay of a current ring and as it decays it ejects hot dense plasma in jets that propagate axially from each side. It is within the axial jet that the material samples will be positioned. FRC's are typically created in a low pressure environment where fuel gas pressures can be controlled and contaminants are in low concentrations. The creation of an FRC plasmoid requires the existence of sufficiently ionized and uniform base plasma for trapping the soaked in reversed bias flux.

Shown in Fig. 3 are the design of the FRC test bench and a real image of the fully constructed system. The FRC chamber, where the plasmoid is formed, is a 10 cm ID, 60 cm long, quartz tube purchased from Hayward Quartz Technology Inc, and is centered between two ISO 100/NW 50 stainless steel four way crosses that support the experiment and provide ports for pumping and plasma diagnostics. The chamber is pumped out by two mini Boc Edward turbo pumps that maintain a base pressure in the mid 10^{-7} Torr and are electrically isolated from the formation chamber by quartz nipples. The background pressures are monitored with standard thermocouple and cold cathode gauges and contamination profiles with partial pressures are measured using an SRS Residual Gas Analyzer (RGA) 100. Multi-turn, solenoid cusp/guide coils are positioned on each side of the FRC formation chamber to both aid in the formation of the closed magnetic field line profile, and guide the plasma jet onto the sample. The capacitor charge voltage and related field strengths can be adjusted to vary the exposure intensity onto the target. These guide coils are typically driven at ~750 V and ~165 Amps with a 1.2 mF capacitor bank having a rise time of 4 ms. This configuration produces a magnetic field strength of approximately 0.2 Tesla. The sample is placed on the end of a standard 4 foot long Ultra High Vacuum (UHV) magnetic translation arm and can be positioned anywhere within the guide coils. On the side opposite from sample insertion, a Pre-Ionization (PI) gun is positioned. The PI gun is used to aid in the creation of uniform pre-formation plasma within the chamber and is currently operated at 4kV with a local deuterium gas pressure of ~10 mTorr. The quartz tube making up the formation section is surrounded with eight single turn copper coils in a theta-pinch configuration that fit snugly around thin polyethylene shims. Each shim and each coil are individually wrapped with an electrically isolated copper wire loop that will be discussed in the diagnostics section.

The coils are driven by three independent capacitor banks arranged in a parallel circuit configuration as shown in Fig. 3; the main formation bank (C_F), ringing-θ (C_R) and bias bank (C_B).

The formation bank is comprised of eight 1.85 µF capacitors each equipped with a 25kV copper-vapor thyratron start switch capable of sub-microsecond triggering resolution. Each start switch is paired with a crowbar switch (CB) that is triggered at peak current, allowing the magnetic field external to the FRC (B_e) to remain relatively constant after formation. Each formation capacitor is capable of delivering 150 kA to each coil, generating magnetic field magnitudes on the order of 1 Tesla. The ringing-θ bank is a 1.8 µF capacitor connected in parallel the eight formation coils and is operated at 22 kV delivering a ~1 MHz frequency oscillating field profile during pre-ionization. The bias bank is 120 µF inductively isolated (by L_B in Fig. 3a)) capacitor operated at 4kV providing a 0.1 – 0.2 Tesla negative bias field. Charging of the capacitors is monitored through independent voltage to frequency monitors coupled to a charge control system controlled with LabView. Fuel gas is pumped into the formation section through fast gas-puff valves with temporal resolution on the order of microseconds. The fuel gas is injected into the chamber via the PI gun. Gas pressures are accurately measured using a capacitive monometer positioned on the end of the formation section opposite the end where gas is introduced.

II.e Experimental Operation

The pre-ionized fuel gas to be used during the generation of the FRC plasmoid is created through the combination of a bias and ringing field pattern. Fuel gas is pumped into the chamber in two steps; the first puff is timed to fill the chamber to a sufficient fuel gas pressure required for plasmoid formation, fill pressures are typically on the order of 10 mTorr. The second puff is timed
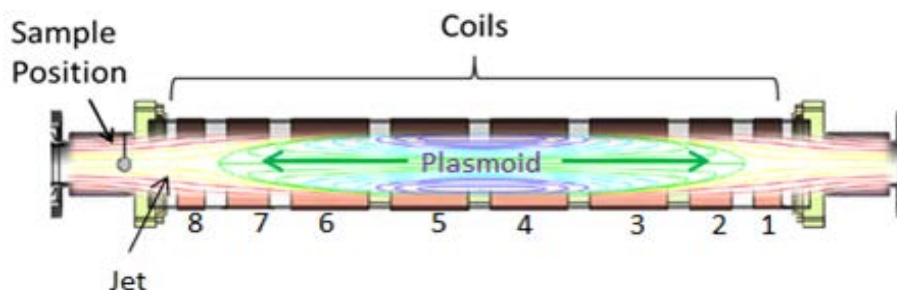

Figure 4: CAD drawing of formation section including eight single turn copper coils with expected magnetic field contour lines. The sample position is also indicated here.

to fill the PI gun with enough gas to allow a Paschen breakdown between the gun electrodes at 4 kV. The bias sets the initial direction of the field. The PI gun is then fired providing seed plasma to the formation area. At the first quarter cycle of the bias, the ringing-θ is triggered producing field oscillations that briefly swing the bias field down to zero amplitude to further ionize fuel gas. The formation coils are then triggered rapidly and with the opposite polarity compressing the plasma and reversing field lines resulting in the creation of a closed field plasmoid. As the plasmoid decays, hot ions flow off the plasmoid, into a jet that streams axially through the guide coils and onto the material target. Figure 4 illustrates the formation section with expected magnetic field profile during plasmoid equilibrium. The coils on the ends are of reduced width as a method of increasing the current per unit length to compensate for the lower magnetic field at the end of the solenoid and provide a slight mirror field to aid in FRC confinement. The triggering times for the various components of the formation process are critical and in some cases require sub-microsecond scale timing. Figure 5 shows the current firing times for the different components of the system that result in the formation of a stable FRC. Noise that could result in a misfire is

Capacitor Banks	Capacitance	Charge Voltage	Risetime	Time of Trigger	Field Strength
Guide coils	1.2 mF	750 V	4 ms	-4 ms	0.261 T
Pre-ionization	14.7 μF	4kV	6.5 μs	-30 μs	N/A
Reversed Bias	122 μF	4.5kV	15.7 μs	-26.8 μs	-0.09 T
Ringing-θ	1.8 μF	22kV	1.1 μs	-8.5 μs	0.1 T
Formation	1.8 μF x8	20kV	1.2 μs	0 μs	0.8 T

Figure 5: Values for operational parameters of capacitors used to create magnetic field profiles necessary for plasmoid creation. Formation bank includes eight independent capacitors coupled to their own independent copper coils. Triggering times are in relation to the formation triggering time being set to zero seconds.

mitigated by extensive use of optical fibers and custom made switches with high temporal resolution. The triggering time for each coil can be controlled and tuned independently for optimum conditions and all controls are maintained through a custom LabView VI panel. Through the VI panel all aspects of device operation can be automated, including; charging and voltage monitoring, triggering, data acquisition, as well as a continuous operation mode.

II.f Plasma Diagnostics and Plasma Behavior

The material studies require that the plasma source be well characterized to relate material damage to plasma energies and fluence. This plasma source is characterized through the combination of several fundamental techniques commonly used to measure plasma characteristics. The primary diagnostic technique, a compensating flux loop array, involves the placement of two copper wire loops positioned on the inner and outer circumference of each coil. Using the current driven in each wire loop during magnetic compression, the excluded flux ($\Delta\phi$), and excluded flux radius (r_s) of the plasmoid can be measured and calculated using the following expression [11].

$$\Delta\phi = \pi r_l^2 B_e - \phi_l = \pi r_s^2 B_e \qquad \text{Eq. (1)}$$
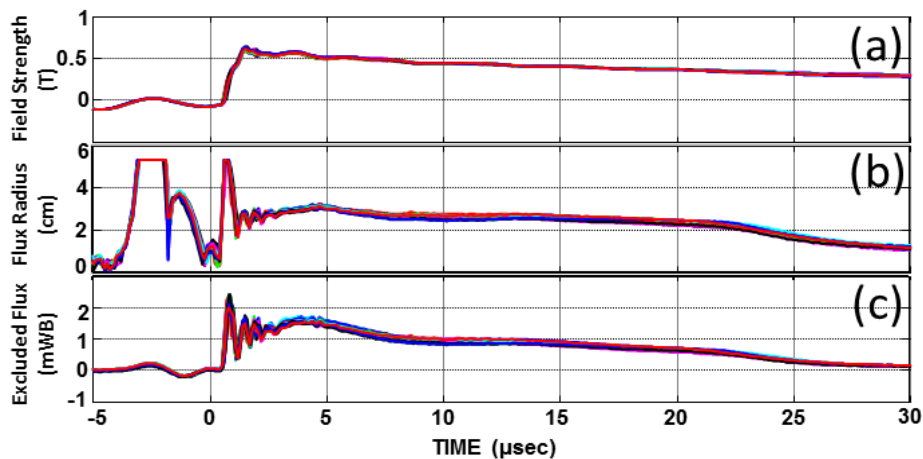

Figure 6: Measurements from coil number 5, (a) magnetic field strength, (b) excluded flux radius and (c) excluded flux field strength during plasmoid generation.

8

Here the loop surrounding the OD of the coil measures the total flux (ϕ_l), whereas a crescent shaped loop surrounding the polyethylene shims measure the portion of flux that is compressed against the coils as the plasmoid is formed (B_e). Figure 6 is an example of measurements taken from compensating flux loops on coil number 5, which is roughly in the center of the formation section. Graph (a) shows the magnetic field strength, (b) is the excluded flux (plasmoid) radius and (c) the excluded flux field strength. It can be seen that over the course of 15 consecutive shots the magnetic field and plasmoid excluded flux conditions remain highly consistent and give rise to a plasmoid cross sectional radius of ~3.5 cm with a life time of on average ~25 μsec. From the data collected on all coils it was determined that the plasmoid lengths are averaging approximately 40 cm. It was observed that these conditions can be further sustained over the course of hundreds of shots.

With the plasmoid radius known, a Michelson Interferometer was used to measure the density of plasma in the center of the plasmoid. One beam of the laser is passed through the formation section between coils 4 and 5, the reference beam is passed over the top of the coils and back to recombine with the first beam where the co-linear beams constructively and destructively interfere depending on their relative phase shift. From the change in phase ($\Delta\phi$) between the split beams the plasma density can be calculated using the following relation [14].

$$\Delta\phi = \frac{\omega}{2cn_c} \int n_e dl \qquad \text{Eq. 2}$$

where ω is the angular frequency of the laser, c is the speed of light, n_c is the cut-off density related to the index of refraction, dl is the path length through the plasma or in this case the cross sectional diameter of the plasmoid, and finally n_e is the electron density which for deuterium is equal to the ion density. By employing this technique, it was determined that plasma densities are averaging ~$5 \times 10^{21} \, m^{-3}$ at 10 μs during the equilibrium phase. In addition, from the density and field measurements it was determined that the plasma temperatures are averaging ~130 eV.

Traditionally ion velocities are measured with a Langmuir probe. However, because the ion energies far exceed the work function of valence electrons within tungsten probe material a Langmuir probe may not yield accurate information to determine average ion velocities within the plasma jet.
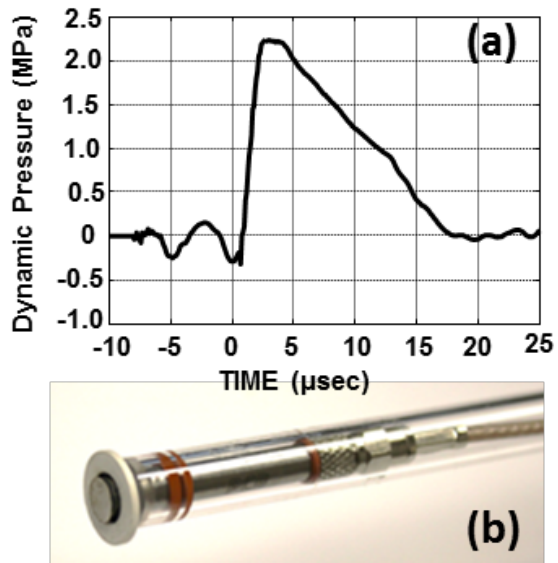

Figure 7: (a) Typical Pressure vs. Time plot for dynamic pressure wave of plasma jet. (b) Real image of probe inside quartz tube with boron nitride annulus surrounding the sensing surface.

9

Following a previous design, outlined by S.J. Messer et al. [15], a novel design making use of a dynamic pressure probe was used to measure ion velocities in sample exposure positions within the plasma jet. The probe utilizes a PCB Piezotronics model 113B21 pressure sensor modified to work in the plasma jet environment. The entire probe was housed within a 1 cm OD, 0.7 cm ID, 122 cm long quartz tube using a low vapor pressure epoxy for a vacuum tight seal. The probe was positioned in the tube such that the sensor end protrudes from the end of the tube approximately half of a centimeter. The sensor itself has a stainless steel casing; therefore, it was necessary to isolate the protruding part of the probe from the conductive plasma by applying a thin layer of epoxy around all exposed surfaces. A boron nitride annulus was positioned around the end of the quartz tube to allow the sensor end to be exposed directly to the plasma while protecting the epoxy seal from the plasma jet. Additionally, tungsten foil was attached to the leading edge of the sensor with an extremely thin layer of epoxy to absorb the
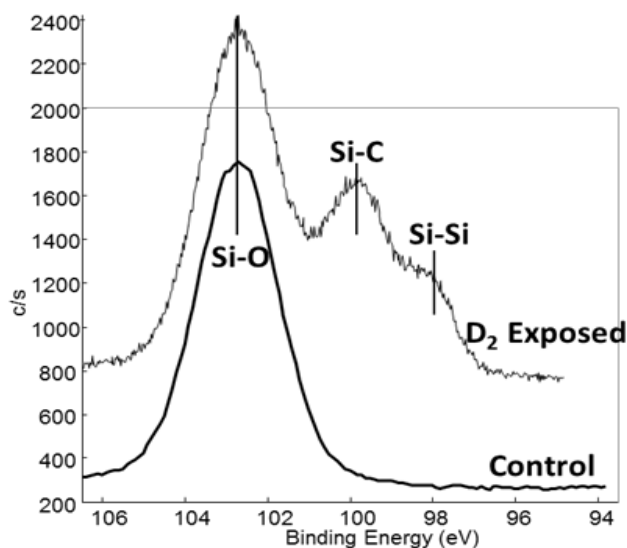

Figure 8: X-ray photoelectron spectroscopy results from Macor target before and after deuterium plasma exposure. The control samples shows 100% oxidation of silicon constituents whereas the exposed sample clearly shows the addition of carbide and silicon segregation on the surface.

direct energy of the plasma without damping the sensitivity. Figure 7 illustrates the probe and corresponding dynamic pressure waveform during operation. The sensor was tested before and after the modification and it was determined that there was no sufficient change necessary in the factory calibration of 3.6 mV/kPa. The relation between pressure and ion velocity is expressed by the following:

$$P_0 = n_0 kT = 0.5\rho v^2 \qquad \text{Eq. 3,}$$

where P_0 is the pressure, ρ is the mass density of a deuterium ion, and v is the ion velocity. As a result, measurements indicate dynamic pressure readings on the order of 1MPa at 10 µs which translate into ion velocities on the order of ~300 km/s at the sample exposure position.

X-ray photoelectron spectroscopy (XPS) was employed in an attempt to map the structure of the plasma jet in sample exposure positions. It has been seen in our previous studies through extensive XPS analysis that deuterium plasma has sufficient energy to facilitate carbon-silicon bonding on the plasma facing surface of silicon rich Macor samples [16]. These studies showed that atmospheric carbon deposited on the surface of Macor samples before insertion into the FRC chamber resulted in a substantial formation of silicon carbide. Therefore, a flat Macor disk was polished, and prepared for deuterium exposure by sonicating the sample in both methanol and isopropanol for 15 minutes each. The sample surface was allowed to be exposed to atmosphere before being placed into the FRC chamber allowing for a uniform thin film of atmospheric carbon contamination to be deposited onto the surface. Figure 8 is an example of the XPS surface scans

comparing the unexposed control sample of Macor with the deuterium-irradiated sample. It can be seen that in the control sample the silicon exists only in the oxidized state, however the deuterium exposed sample shows the addition of two distinct new peaks. One at the binding energy of 99.8eV, a characteristic binding energy for silicon carbide, and another at 98.0eV implying some silicon segregation has occurred on the surface as a result of the exposure. It was proposed that during exposure the variance in the energy cross section of the ion beam should result in an identical chemical pattern of silicon carbide formation on the Macor surface. Therefore, extensive XPS and depth profiling analysis was performed by scanning a cross section of the Macor sample surface after exposure. Analysis focused primarily on the Silicon 2p peak. Specifically, the percentage of oxide, carbide and silicon segregation was measured at 2 mm intervals across the sample surface. Results from the analysis can be seen in Fig. 9. It appears that the silicon carbide is most prevalent in the center of the sample and is consistent with the visible discoloration at the samples center. The variance in the chemical percent was low in the central 1.2 cm of
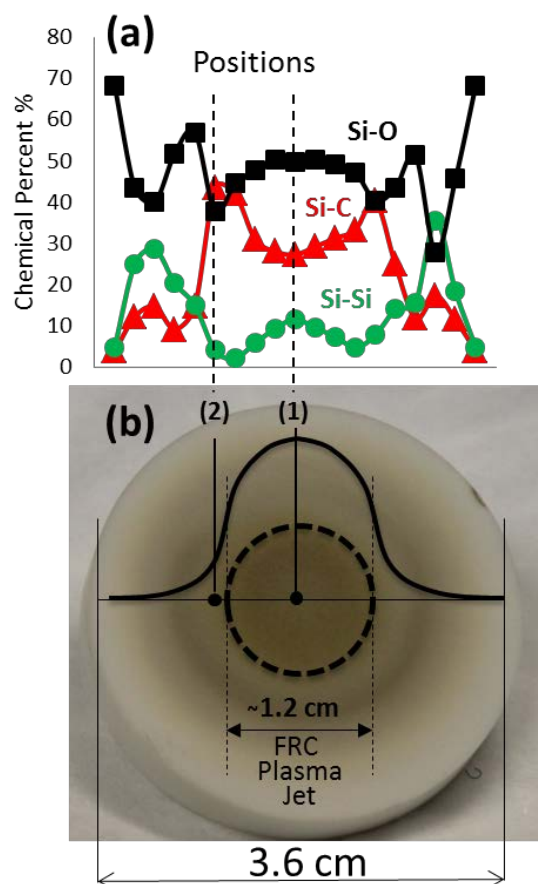

Figure 9: (a) XPS surface analysis of chemical percentages in the silicon 2p peak and (b) Macor target with circular discoloration patterns associated with the deuterium plasma jet and superimposed Gaussian beam structure.
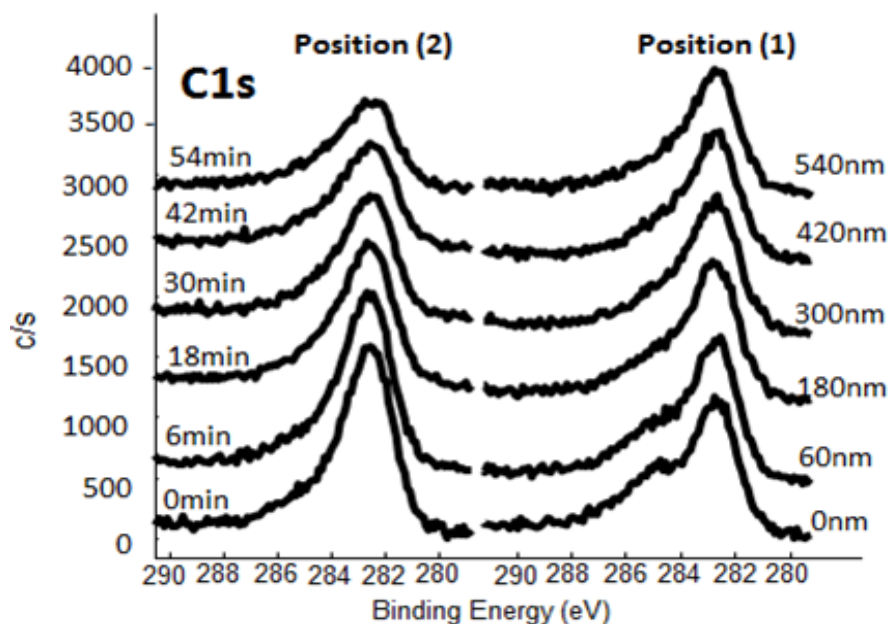
the sample and a sharp increase of silicon carbide was detected at the edges of this central region. XPS depth profiling was then conducted in the center position and at the edge of the 1.2 cm structure with a low energy argon sputtering technique. Analysis of the depth profiles focused on the carbon 1s peak.

Figure 10 illustrates the results from the depth profiling of the center (position 1) and the outer edge of the inner ring structure (position 2). It appears that the carbide in the center position was more persistent and harder to remove than the outer edge implying a deeper penetration of carbon into the material from a more energetic region of the plasma jet. The edge of the inner ring structure shows a higher percentage of carbide, but was easier to remove which would be more consistent with a carbide deposition from the sputtering of the center during the exposure. As a result the size and structure of the plasma jet could be mapped at a spacial resolution of 2 mm. Theoretically, the resolution could be as low as the XYZ axis manipulator resolution on the stage of the XPS which is less than 0.5 mm. Figure 9(b) is an image of the Macor disk after 100 shots and clearly illustrates the circular and symmetric nature of the plasma jet with the superimposed results of the plasma

Figure 10: XPS depth profiling results. Center (position 1), outer edge (position 2). Indication that in the center position the carbon atoms where driven deeper into the material resulting from higher plasma jet energies.

beam energy profile from the XPS depth profiling study. It was concluded that the beam structure was Gaussian with a FWHM of approximately 1.2 cm.

II.g Experimental Device Summary

A small scale FRC plasma source was created for the purpose of conducting high density plasma-material interactions studies. The source is well characterized with a robust design and highly repeatable conditions over multiple shots. Plasma densities are roughly 5×10^{21} m^{-3}, average ion velocities of approximately 300 km/s, and kinetic energies ranging from 10 kJ/m^2 to 1 MJ/m^2. XPS depth profiling analysis revealed a Gaussian plasma jet structure approximately 1.2 cm in diameter propagating axially through the guide coils. Future plans to further equip the facility include the addition of an Auger spectrometer for in-situ chemical and depth profiling analysis, thermal desorption spectrometer to measure fuel gas desorption rates and a plasma induced thermo-calorimetry detector directed at the sample surface during exposures. These future characterization tools will further enhance the overall design of the plasma-materials research test bed and provide a unique opportunity to study the many effects of high energy high fluence plasma exposures on solid state materials.

II.h Materials Characterization

The samples were observed before and after exposure of plasma using both optical microscopy (OM; Olympus B51X Microscope, Center Valley, PA) and Scanning Electron Microscopy (SEM; JEOL JSM7000 SEM, Peabody, MA). In this context, OM and SEM imaging were deployed as a tool to provide a visual representation of the resultant degree of sputtering and re-deposition of the samples as well as Macor® holder. X-ray photoelectron spectroscopy (XPS; PHI-VersaProbe, Chanhassen, MN) was used to identify which elements and relative amounts were re-deposited onto both the samples and the Macor® holder. The chemical compositions of depositions were also determined, and the relative thickness of the deposition layers as a function of sample height was clearly indicated through XPS analysis with an argon sputter depth profiling method. A nominal sputtering rate calibrated by SiO$_2$ was ~10 nm/60 s when the Ar beam energy was 1 keV with a beam current of 1 μA while rastering over 2x2 mm^2 area. The information obtained through OM, SEM, and XPS were used to develop a qualitative and quantitative model dictating the importance of position within the chamber on sputter and re-deposition phenomena.

The experiments were carried out ex-situ, where samples were exposed to atmosphere before and after deuterium exposures. The consequent contamination of atmospheric gasses provided a source of carbon; however, due to the presence of oxygen in the Macor®, atmospheric contamination of oxygen would have played a less significant role on the chemical nature of the post exposed samples.

III. RESULTS

III.a Compositional changes of Macor® surface induced by plasma irradiation

Macor® is a commercial ceramic material with the composition of 46wt % SiO$_2$, 17wt % MgO, 16 wt% Al$_2$O$_3$, 10 wt% K$_2$O and 7 wt% B$_2$O$_3$ with 4 wt% F [16]. Addition of ionic fluorine in the composition results in the high machinability; thus the Macor® is used to fabricate various designed components in our experiments. Of particular interest are the effects that a high energy deuterium plasma has on various materials, and some of this information can be gained from the

redeposition of materials seen on the Macor® sample holders themselves. For this, we first looked at compositional changes of the Macor® surface induced by irradiation of transient plasma.
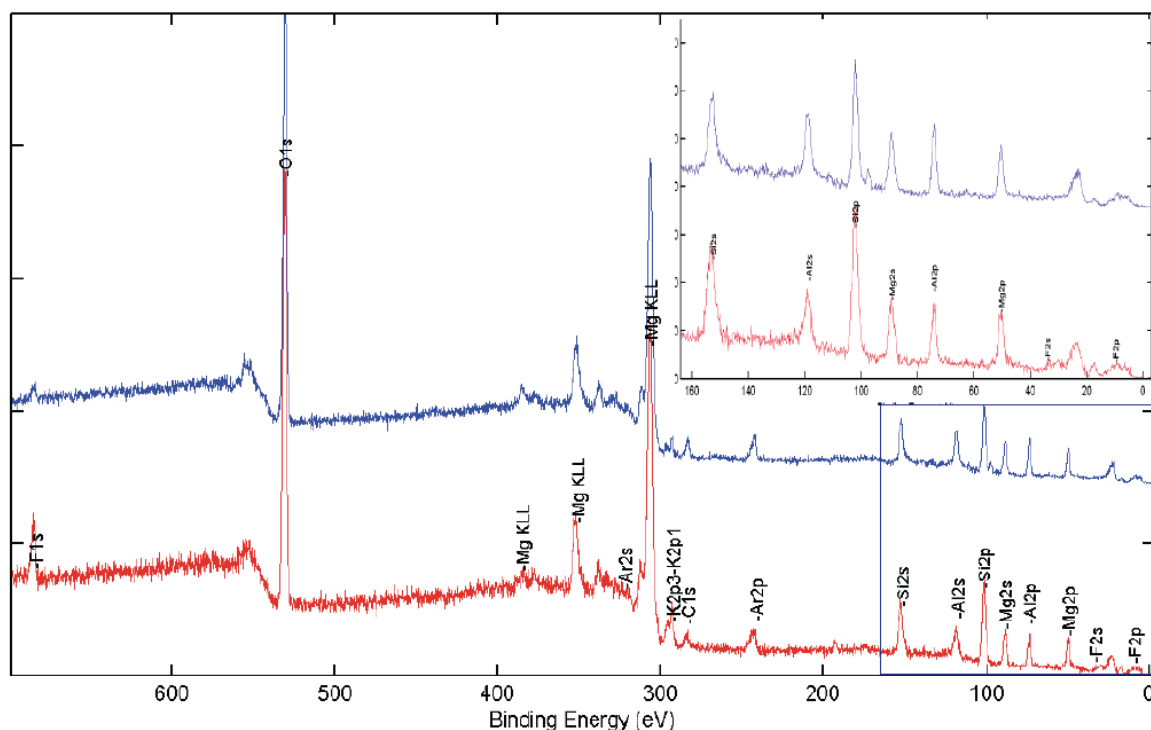

Figure 11: XPS spectra of the Macor® surface before (red) and after (blue) plasma irradiation.

Carefully comparing x-ray photoelectron spectra of the Macor® surface before and after plasma irradiation, two features are evident in Fig. 11; removal of fluorine peak and significant reduction of Si 2p and Si 2s peaks as seen by the evolution of shoulder peaks in the lower binding energy. These two effects can be considered to be two distinct but interrelated effects, the former leading to the latter. Under repeated exposure to the deuterium plasma, high kinetic energy deuterium ions repeatedly impacted and penetrated the surface of the sample. It is not unreasonable to expect that the chemical bonds would be broken, in similar manner to a more standard ion beam exposure. It is therefore plausible that some of the oxygen could react with the hydrogen, forming water, which would easily be removed from the system. The bond energy of Si-O bonds in SiO_2 is approximately 6.44 eV / atom [17], a relatively low value which could easily be overcome by high kinetic energy particles. Also important to note, the Si-Si metallic bond energy is 3.38 eV per atom [17]. As a brief but important aside, the bond energies of MgO, K_2O, and Al_2O_3 are much higher than that of the Si-O bond. This explains why there is no obvious dissociation of the Mg, Al, or K peaks like there is of the Si 2p and 2s peak.

In essence, the exposure to plasma had a reducing effect on the surface, removing some oxygen, and leaving metallic silicon. It has been widely seen that metallic silicon has been readily etched by fluorine ions, due to exposure to fluorine containing gases [18, 19]. Additionally, F- ions in a material can penetrate deep into the material, due to the high mobility of the small, unreactive, highly electronegative ions [20]. The etching reaction between active F- ions and metallic Si results in the creation of fluorosilane [18, 19, 20]. Some of these gaseous species completely desorb

14

from the surface, causing removal of material [18] but some remains adsorbed. Additionally, as metallic Si bonds are replaced over time by Si-F bonds, there will be intermediate species of the form SiF_x where x = 1,2,3,4 [18, 19, 21]. When x = 4, the compound is the gaseous species, known as tetra-fluorosilane. It is important to note, that fluorine will *not* readily react with SiO_2 to form SiF_x compounds [19]; rather, some way of breaking bonds and supplying the activation energy for formation of SiF_4 must be supplied. The free energy of formation of SiF_4 is about 16.3 eV per atom [20], an amount that could easily be supplied due to plasma exposure. The plasma exposure could also supplied energy to cause rapid desorption of SiF_4, potentially increasing the rate of said reaction [19].

The interaction described above is what is known as chemical sputtering [22]. This is the effect of sputtering interactions providing the necessary energy for a reaction to take place the otherwise would be highly kinetically limited. In this case, the kinetic energy transfer, in addition to simply removing material, gave energy to form tetra-fluorosilane, *and* then further desorb the gas, preferentially removing silicon and fluorine from the surface of the sample. Each time a SiF_4 molecule is removed from the surface, 4 F- are removed, and only one Si is removed. This, coupled with the high mobility of F- ions, *and* the concentration gradient arising from the removal of F- from the surface and near surface region, explain the complete lack of a F1s peak in the above spectrum. There is a large amount of Si in Macor®, even with metallic Si being preferentially removed due to chemical sputtering. There is relatively little F; however, it is not at all unreasonable to expect to see no F1s peak, and still see a small Si peak at a lower binding energy corresponding to metallic Si bonds.

The removal of F from the surface is significant, because the presence of F- ions in the Macor® gives the machinability to the material. Without it, the material would respond similarly to other brittle ceramics during processing, potentially cracking and undergoing fast fracture. This removal of fluorine has implications for the survivability of the Macor® sample holders after several exposures to deuterium plasma, as embrittlement and possible fracture due to thermal cycling stresses etc., could cause failure in the holder and compromise experiments.

III.b Effects of geometry on sputtering and re-deposition dynamics

Tungsten (W) pellets and Macor® were used to gauge the effect of sputtering and re-deposition during plasma exposure. Each tungsten pellet was placed into the Macor® sample holder at different depths and heights relative to the holder surface. Two pellets were recessed into the holder at -1/16" and -1/32", one sample was flush and one slightly above the surface (<+1/32"), and three above the surface at +1/32", +1/24", +1/16". Shown in Fig.12 and Fig. 13 represents the optical microscopy (OM) images and x-ray photoelectron spectra of the tungsten samples taken after exposure was completed, respectively. It is clearly seen that there is a substantial difference in the physical appearance, where the re-deposition of Macor® appears to be more pronounced on the W surfaces that are above the Macor® holder surface.
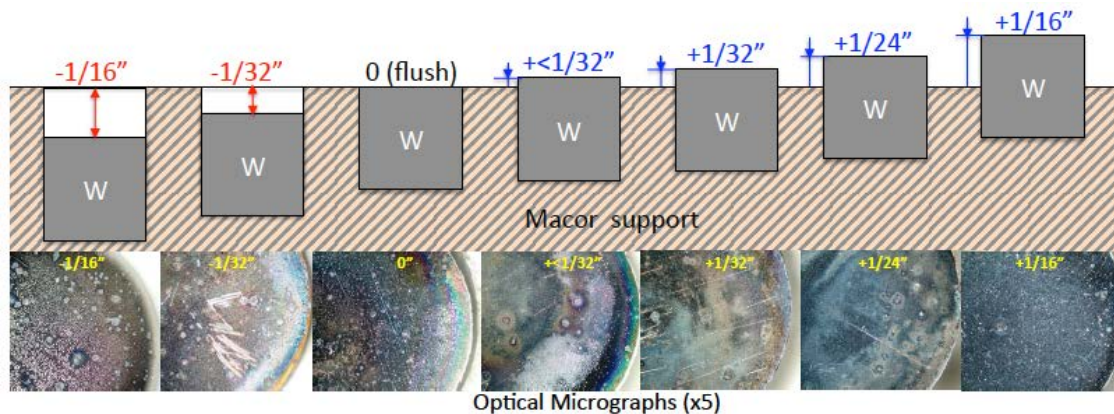
**Figure 12: Optical microscopy (OM) images of the tungsten samples placed into the Macor®
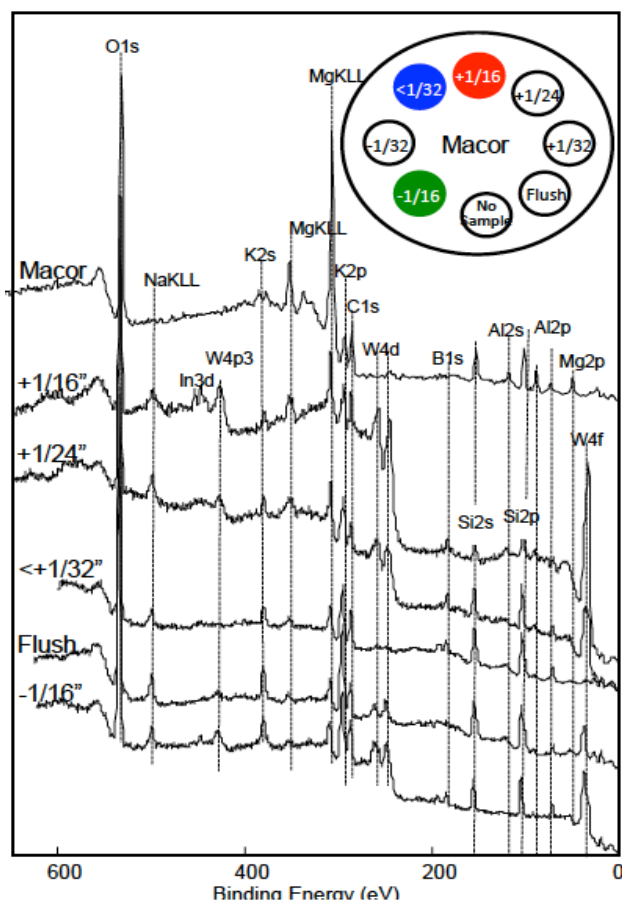sample holder at different depths and heights relative to the holder surface during plasma exposure.**

**Figure 13: XPS spectra of the tungsten samples placed into the Macor® sample holder at different depths and heights relative to the holder surface during plasma exposure.**

XPS analysis from each surface reveals that all elements from the Macor® were shown. XPS depth profiles for selected elements (W, Al and Si) from the samples located at three different heights (+1/16", <+1/32", and -1/16") are shown in Fig. 6 to reveal the chemical changes of the constituents within sub 10's nm depth from the surface.
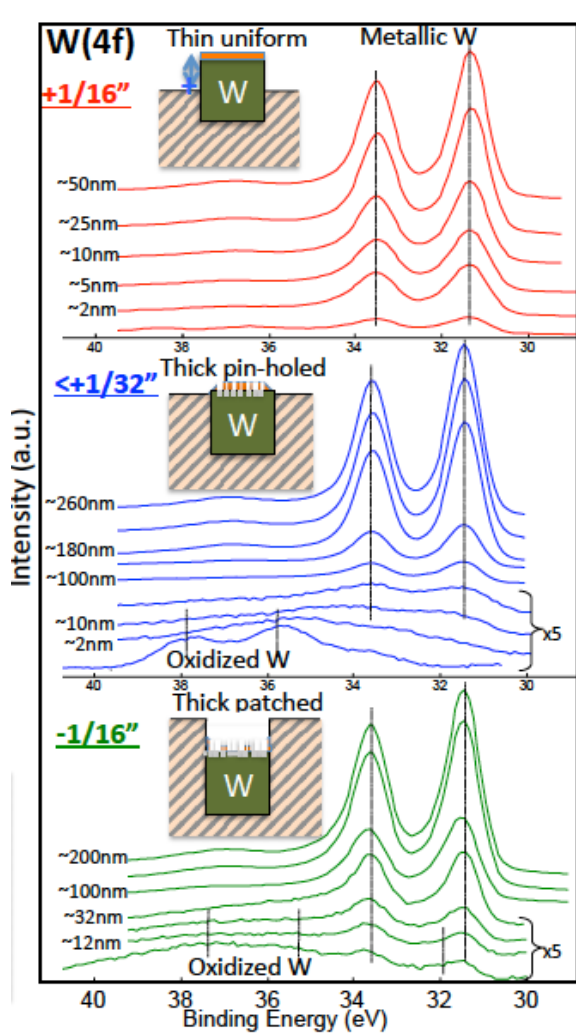
(a)

(b)

(c)

Figure 14: XPS depth profiles for selected elements (W, Al and Si) from the samples located at three different heights (+1/16", <+1/32", and -1/16").

The tallest sample (+1/16") in the XPS scan showed the presence of constituents from both the substrate (W) and Macor® (Al, Si, Mg); however, the chemical state of W remained as metallic and was not oxidized throughout the depth profile as shown in Fig 14(a). This indicated that the sample was entirely covered by a thin deposition of Macor® film whose thickness was less than the standard photoelectron sampling depth of a few nm. The OM image (Fig. 12) showed roughness resulting from the erosion caused by the plasma interactions; however, the eroded layer was both physically and chemically modified to the depth of ~10's nm as discussed below.

The next tallest sample at +1/24" is starting to show visual signs of discoloration due to deposition of Macor® material. Among those, the sample that was just above the surface (<+1/32) is visually the most extreme in discoloration, as indicated by the intense coloration the sample, where a heavy deposition took placed around the perimeter of the sample and was tapered off in thickness toward the center. The flush sample also shows strong visible signs of the Macor® re-deposition, where the heavier deposition around the perimeter was again tapering off toward the center. Looking at the XPS survey scans from nearly flush samples (<+1/32" and flush), there is none or only a small tungsten signal, indicating that the thin film layers re-deposited from the

Macor® substrate became thicker, hindering the appearance of W signals from the surface. A high resolution W spectra from these samples showed marked oxidation of W at the surface (Fig. 14(b)); however, it becomes metallic, coexisting with other Macor® elements in the sub-surface region. The negatively recessed sample (-1/16") shows an interesting result, where lesser amount of Macor® re-deposition took placed, which was rather unexpected. In this sample the visual appearance was noticeably different than the exterior samples, where the deposition appears to be much thicker in the center than at the perimeter, suggesting that the negatively recessed sample would restrict the plasma flow to the center due to the walls.

Although the physical appearance of morphology greatly differs with different sample heights, the chemical nature of the thin films and their subsurface structure share similar trends. Re-deposited Macor® thin films on the W samples consist of all elements found in the Macor® substrate (See Fig 11, Macor® reference spectrum); however, the relative thickness of each deposition is significantly different. Of most elements, Si and K are the most pronounced constituents in the re-deposited thin films, whereas Al and Mg are present in the least amount. A height dependent sputter and re-deposition phenomena observed above is schematically drawn in Fig 15.
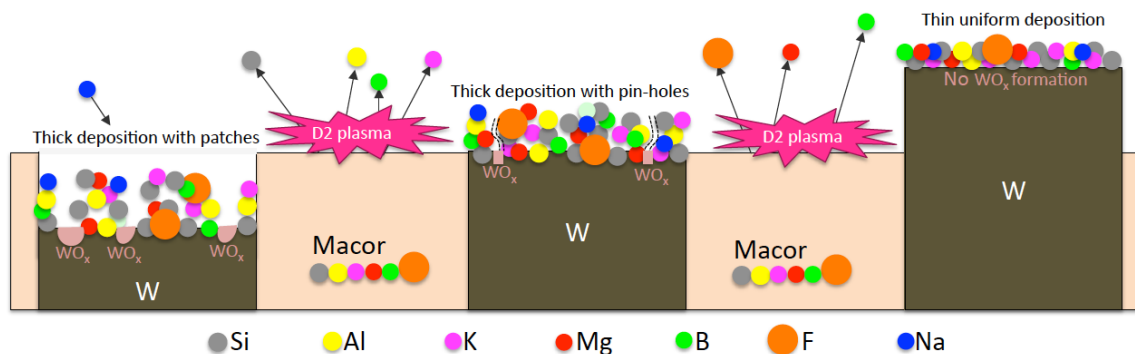

Figure 15: Schematically illustrated height dependent sputter and re-deposition phenomena.

Another significant effect is that the Al species originating from the Macor® and re-deposited on the W appeared to be reduced as evident from the peaks appearing at the lower binding energy side in Fig 14(c). Appearance of the metallic Al species is rather surprising since the free energy of formation for the Al-O bond is large, so that the bond should be stable even under the extreme conditions; however, the situation is obviously different in this case. Although this unexpected thermodynamic effect influenced by plasma-wall interactions is still unknown, it is commonly known that the alumina, after prolonged plasma exposure, exhibits sizable electrical conductivity on the surface, implying that Al_2O_3 is heavily reduced to form metallic Al layers on the surface. The present results are at least consistent with this observation, however, further investigation to elucidate this phenomenon is needed in the future.

III.c Chemical and Morphological Interactions with Cu, Al, Ti, Zr and W.

The second study was conducted to evaluate chemical and morphological effects of various metals exposed to deuterium plasma. In this study Macor® was again employed as the sample holder. The samples included copper, aluminum, tungsten, titanium, and zirconium. Figure 16 is a

photograph taken right after exposure and illustrates the sample configuration. In this experiment the tungsten (W), copper (Cu), and zirconium (Zr) samples were set at two heights relative to the holder surface for both a strong and weak interaction with the Macor®. There was only a single sample of both aluminum (Al) and titanium (Ti) set at intermediate heights. The Al sample was visibly the most damaged by the exposure. OM images confirmed the presents of well rounded edges and large cracks on the surface of the Al sample. The Ti sample was visibly the least affected by the exposure. Later XPS analysis of the Ti sample indicated that a thick deposition of Zr had been deposited on the surface with little presence of Macor® material.
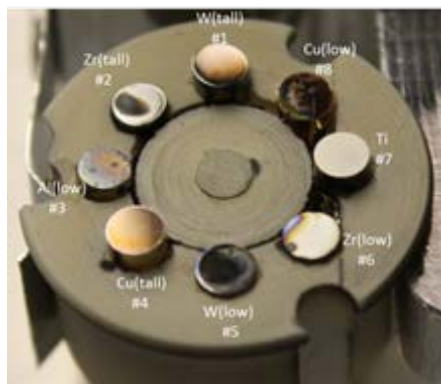

Figure 16: A photo taken immediately after exposure of W, Cu, Zr, Al and Ti described in text.

Scanning Electron Microscopy (SEM) was used to further explore the morphological effects of the deuterium exposure on the plasma facing surfaces. Shown in Fig. 17 is a collection of SEM images from the Cu, Al, W, and Zr samples observed at 2500 times resolution. For comparison, OM images are also embedded in the figure.
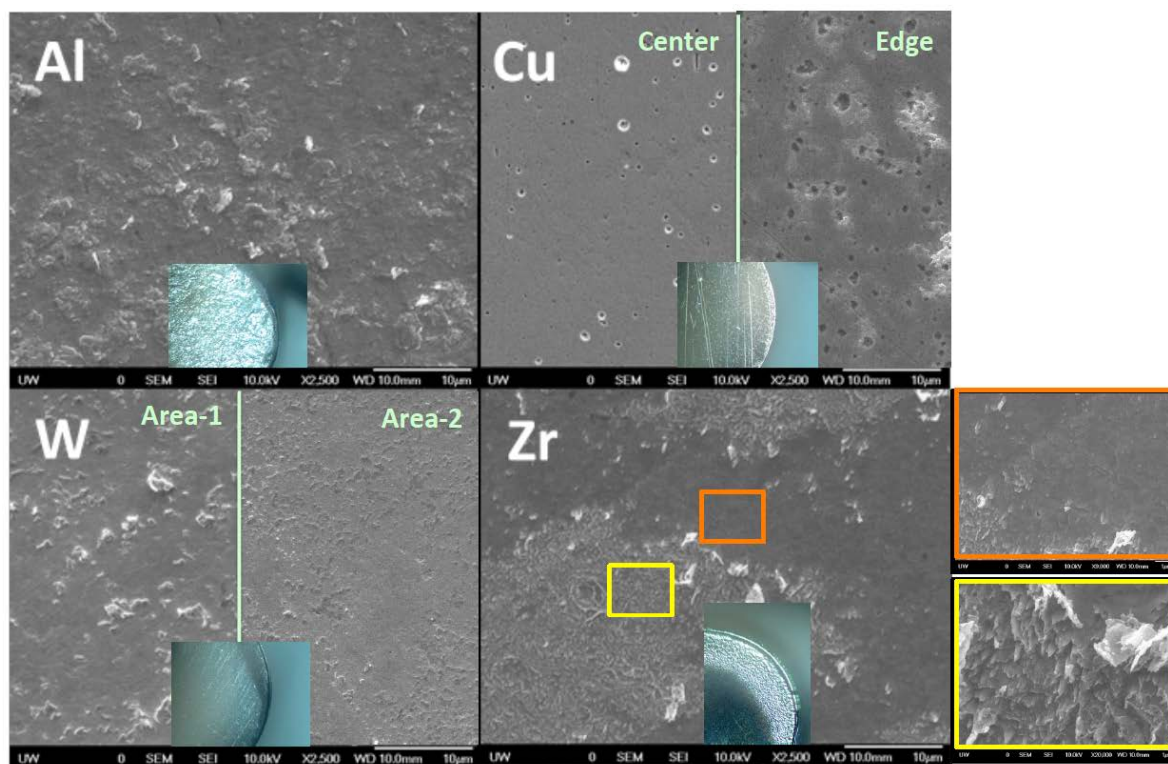
Figure 17: SEM images from the Cu, Al, W, and Zr samples at 2500 times resolution. OM images are also embedded for comparison.

The Al and W samples have a similar morphology in that there seems to be a rather uniform pattern of oxide formation. EDX was used to confirm that the formations are in fact oxides; however due to the presence of oxygen in the Macor, it is unknown as to whether the formations oxidized during the irradiation or upon exposure to atmosphere. The Cu and Zr samples have a rather unique morphology. The Zr sample has a non-uniform visible appearance. The darker regions indicate a smother surface whereas the lighter regions are considerably rougher. Although EDX confirmed the existence of both carbon and oxygen in both regions it was not conclusive to the chemical nature of bonding in both regions. In the case of Cu, the exposure caused micron sized pits to form all over the surface of the sample. Using EDX the pits were found to be copper oxide formations and seem to increase in number toward the edges of the sample. In Fig. 16, how the pitting becomes more pronounced at the edge is illustrated, and is consistent with the deposition findings in part one of the analysis. This would indicate that for protruding elements of the chamber design the edges will experience a significantly stronger physical interaction with the plasma. The image also shows regions of low oxidation (dark region enclosed by circle), and high oxidation (light region enclosed by circle). It is unknown whether this is a direct effect of the deuterium exposure but is interesting that they are essentially side by side.

XPS scans were run on all samples. Depth profile analysis was also conducted, and the results are shown in Fig. 18. As expected, metal surfaces were covered by thin re-deposited films from the Macor substrate; however, their thickness varies as reveled by the Ar depth profile. The "re-deposition model" shown in Fig. 15 can be applied to this case, and these thin-deposited layers from the substrate holder material (Macor in this case) protects metal specimens from further
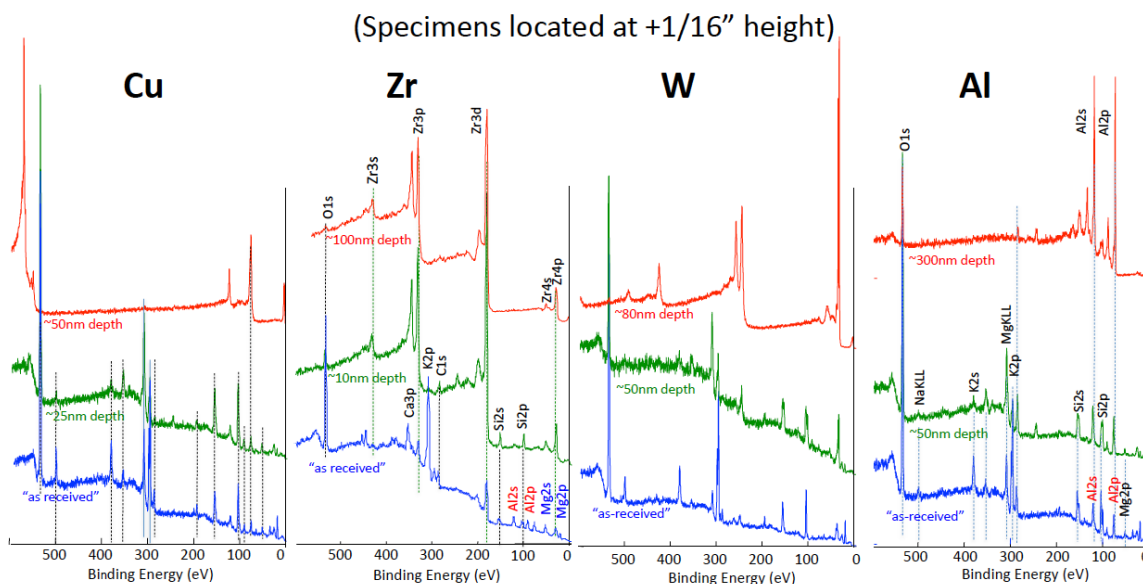
oxidation.

Figure 18: XPS analysis of plasma irradiated Cu, Zr, W and Al specimens. All the specimens were located at +1/16" height from the substrate.

In the case of Zr it was determined that the presence of carbon on the surface of the Zr sample deposited as a result of exposure to atmosphere before the sample was irradiated with deuterium may have resulted in the formation of zirconium carbide. An argon depth profiling study was conducted on the Zr sample. After 5 minutes of Argon sputter (~5nm), the Macor deposition layer was significantly removed showing high intensity Zr peaks that were centered in position consistent with metallic Zr; however, upon inspection of the carbon 1s peak from Fig. 11, it was seen that a small amount of graphitic carbon still remained after 5 minutes sputter as well as a possible zirconium carbide peak centered at 282.1 eV. The NIST standard for C 1s ZrC is between 281.1eV and 282.1 eV [15], this is consistent with our results. It is possible that the exposure to high energy deuterium was the catalyst for the formation of ZrC on the surface of the sample. The sample was further sputtered for a total of 30 minutes and it was observed that the graphitic carbon was quickly removed leaving only the

Figure 19: C 1s region scan of Zr before (red) and after(black) plasma exposure.

carbide that seemed to be highly resistant to sputtering.

III.d Structural variation of ceramic materials before and after plasma irradiation.

Material erosion and deposition, along with the associated long-term fuel retention, are other critical issues for understanding transient plasma-material interactions. There are several distinct mechanisms that would contribute to the diffusion/permeation of plasma fuel in the materials, including bulk diffusion [29], trapping [24], and grain boundary diffusion [25]. In Phase-I of the project, we investigated this phenomenon viewed using an x-ray diffraction (XRD) technique.

Specifically, beryllium oxide (BeO) was exposed to deuterium plasma, and the retention of deuterium was subsequently characterized by calculating the resulting lattice expansion. BeO is a notable electrical insulator with a higher thermal conductivity (330 W/K-m) than any other non-metal except for diamond (its thermal conductivity actually exceeds that of some metals) [18]. In addition, the melting temperature of BeO exceeds 2500 C and its boiling point is 3900 C. Shown in Fig. 12 is the change in the (2-1-13) Bragg peak position from BeO before and after exposure to D_2 plasma. A small shift toward lower diffraction angles indicates that the lattice was expanded by 0.086%. In addition, peak broadening was observed in BeO due to a buildup of intergranular strain. While the shear stress of BeO is around 138 GPa [26], the stress caused by D_2 irradiation is estimated to be ~120 MPa

Figure 20: X-ray diffraction of BeO before and after deuterium plasma exposure.

from the XRD data. This amount of stress is therefore built up by the retention of D_2 plasma fuel in BeO. Continued irradiation may increase fuel retention, leading to the formation of micro cracks when the stress built up in BeO exceeds the maximum tensile strength of ~140 MPa for the material. This crystallography approach is also applicable to other material systems, which could facilitate the attainment of new knowledge with regard to high-density transient type plasma interactions. The strategy will be investigated further in Phase-II of the project.
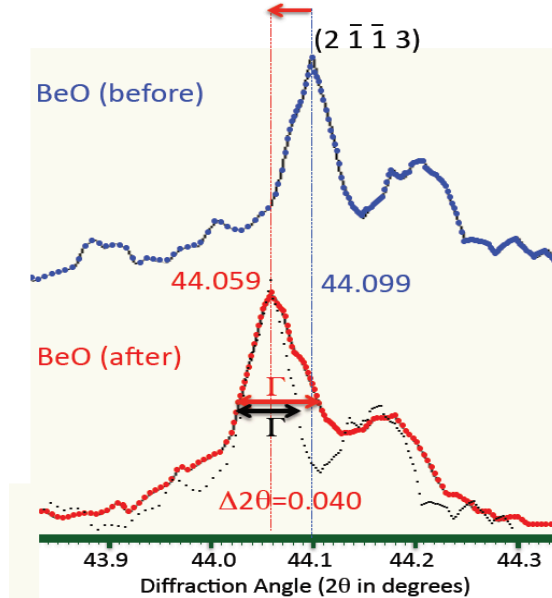
III.D. Preliminary results of Plasma-Wall Interactions from the new FRC plasma facility.

After completion of the new FRC plasma-material testing bench described in **II.b-g**, we tested chemical and physical effects on materials from a transient interaction with non-equilibrium, chemically-reactive, and highly magnetized plasmas. Again, Macor® was used as an indicator to average sputtering and redeposition dynamics for a broad range of the insulating materials.

Upon irradiation of the transient plasma, Macor® surface underwent various compositional changes by preferential removal, sputtering, re-deposition, and dissociation of the constituents. Of particular interest is position dependent evolution of the Si species from SiO_2 containing in Macor® after FRC plasma exposure. As seen in Fig. 21, SiO_2 forms various types of species, including SiC, SiO_xC_y and dissociated Si as well as SiO_2. Interestingly, the amounts of these species vary at different positions of the plasma exposure. At the center of the beam, ~ 50% of SiO_2 of Macor® forms ~30% SiC, ~15% SiO_xC_y and ~5% metallic Si. Outside of the center position, metallic Si is largely suppressed, and more SiC is formed. This enhancement of SiC seems to be due to plasma enhanced reaction of metallic Si with graphitic carbon, of which phenomenon may be unique to the transient plasma conditions. Further moving toward outside of the beam, more metallic Si appeared. This may be as a result of plasma enhanced dissociation of SiO_2. Together with XPS-depth profiling and surface topology analysis, a tentative model of the sputter/re-deposition/evaporation was established as illustrated in Fig. 21. Rich in chemistry as a result of plasma exposure on the Macor® surface can be used to characterize the FRC beam profile with a <1mm resolution. Since none of the conventional plasma diagnostic tools

Figure 21: Compositional variation of the plasma exposed Macor surface.

can resolve this resolution, this is a totally new finding. In Phase-II of the project, we will correlate materials' chemical changes and damages to the plasma parameters listed in Table I, so as to establish the data-base that can be used for the design of future materials that can be sustained for extreme use.
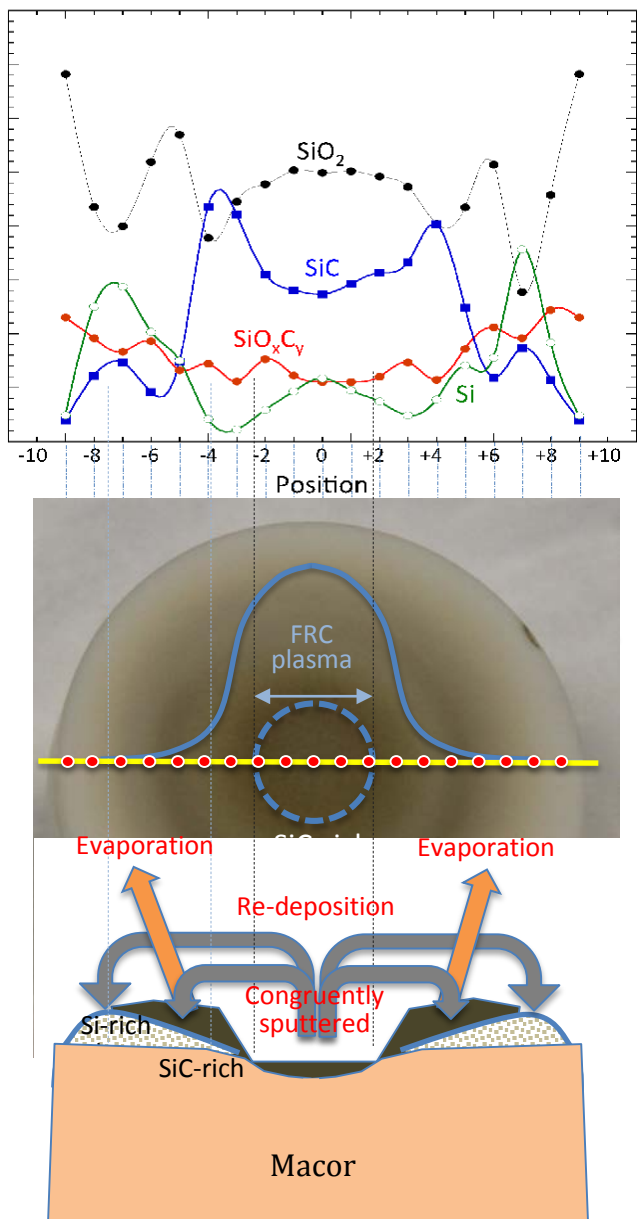
References

1. "Plasma-material interactions in current tokamaks and their implications for next step fusion reactors."G. Federici, C.H. Skinner, J.N. Brooks, J.P. Coad, C. Grisolia, A.A. Haasz, A. Hassanein, V. Philipps, C.S. Pitcher, J. Roth, W.R. Wampler, D.G. Whyte, **Nuclear Fusion**, vol. **41**, p.1967, (2001)

2. "The change of surface topography of plasma facing components in controlled fusion devices." M. Rubel, A. Vevecka-Priftaj, V. Philipps, **Mat. Sci. and Engineering**. vol. **272**, (1), p.174, (1999)

3. "Fundamentals of stationary plasma thruster theory." A. I. Morozov and V.V. Savelyev, in **Review of Plasma Physics**, edited by B.B. Kadomtsev and V.D. Shafranov (Consultant Bureau, New York, 2000), vol. **21**, p. 203.

4. "Quantification of tungsten sputtering at W/C twin limiters in TEXTOR with the aid of local WF_6 injection." S. Brezinsek, D. Borodin, J.W. Coenen, D. Kondratjew, M. Laengner, A. Pospieszczyk, U. Samm and the TEXTOR team, **Physica Scripta T145,** 014016-24. (2011).

5. "Erosion and redeposition of wall material in controlled fusion devices." V. Philipps, P. Wienhold, A. Kirschner, M. Rubel, **Vacuum 67** p.399 (2002)

6. "Plasma–wall interaction: Important ion induced surface processes and strategy of the EU Task Force," Roth J, Tsitrone E and Loarte A **Nucl. Instrum. Methods Sec. B,** vol. **258,** p.253 (2007)

7. "Micro-distribution of fuel and metal in carbon-based plasma-facing materials." P. Petersson, M. Rubel, G. Possnert and B. Pegourie, **Physica Scripta T145,** 014014-19. (2011)

8. MACOR® is a commercial produced by Corning, NY. Specific information about the product can be found at: http://www.corning.com/specialtymaterials/products_capabilites/macor.aspx

9. M.G. Kong, B. N. Ganguly and R. F. Hicks, *Plasma Sources Sci. and Tech* **21**, 3 (2012).

10. T Weber, J. Slough, D. Kirtley, *Rev. Sci. Instrum.* **83**, 113509 (2012).

11. M. Tuszewski, *Nuclear Fusion* **28,** 2033 (1988).

12. L. Steinhauer, *Phys. Plasmas 18, 070501 (2011).*

13. J. Slough, G. Votroubek and C. Pihl, *Nuclear Fusion 51*, 053008 (2011).

14. I.H. Hutchinson, Principles of Plasma Diagnostics. Cambridge: Cambridge University Press, 1987.

15. S. Messer, A. Case, R. Bomgardner, M. Phillips, and F.D. Witherspoon, *Physics of Plasmas 16, 064502 (2009)*

16.   MACOR® is a commercially produced by Corning, NY. Specific information about the product can be found at: http://www.corning.com/specialtymaterials/products_capabilites/macor.aspx

17.   "Chemistry", S. A. Zumdahl, S. S. Zumdahl, 5th Ed., Houghton Mifflin Co. (2000).

18.   "The role of energetic ion bombardment in silicon-fluorine chemistry," J. W. Coburn, H. F. Winters, **Nucl. Inst. and Methods Sec. B**, vol. **27**, (1), p.243 (1987).

19.   "The chemical sputtering of silica by Ar ions and XeF_2." M. A. Loudiana, A. Schmid, J. T. Dickinson, E. J. Ashley, **Surface Science**, vol. **141**, (2–3), p.409 (1984).

20.   "Penetration of fluorine into the silicon lattice during exposure to F atoms, F_2, and XeF_2: Implications for spontaneous etching reactions." H.F. Winters, D.B. Graves, D. Humbird, S. Tougaard, **J. Vac. Sci. Technol. A**, vol. **25**, p.96 (2007)

21.   "IUPAC-NIST Solubility Data Series," J. L. Lyman, T. Noda, **J. Phys. Chem. Ref. Data,** vol. **30**, (1), (2001).

14. "Chemical sputtering, a discussion of mechanisms," H. F. Winters, **Radiation Effects**, vol. **64,** (1-4), p.79 (1982).

15. http://srdata.nist.gov/xps/EngElmSrchQuery.aspx?EType=PE&CSOpt=Retri_ex_dat&Elm=C

16. "Experiments in support of the gas dynamics trap based facility for plasma-material interaction testing", E.I. Soldatkina, A.S. Arakcheev, P.A. Bagryansky, **Fusion Engineering and Design 88**(11) 3084–3090 (2013).

17. "Molecular dynamics study of grain boundary diffusion of hydrogen in tungsten", U. von Toussaint, S. Gori, A. Manhard, T. Höschen and C. Höschen, **Physica Scripta T145** 014036-12 (2011).

18. American Beryllia Inc. 16 First Avenue Haskell, NJ 07420 http://www.americanberyllia.com/BerylliumOxideProducts.html